Geophys. J. Int. (2004) **158,** 470–478 doi: 10.1111/j.1365-246X.2004.02296.x

Core–mantle relative motion and coupling

J. P. Vanyo

Departments of Mechanical and Environmental Engineering, and of Geological Sciences, University of California, Santa Barbara, CA 93106, *USA. E-mail: vanyo@engineering.ucsb.edu*

Accepted 2004 February 27. Received 2004 February 10; in original form 2002 July 29

SUMMARY

Core motion induced by lunisolar precession of the mantle is analysed and compared with experiments and Earth observations. First-order motion has the core axis lagging the mantle axis in precession by a small angle. This misalignment of the axes results in core–mantle relative velocities and displacements over the core–mantle interface as second-order flow. A third-order flow seen in experiments consists of nested fluid cylinders concentric with the core axis. First-order motion can be compared with westward drift and energy dissipation. Second-order motion can be compared with Earth observations using geomagnetic data, although its complexity may require numerical studies for detailed analysis. A specific lag angle and corresponding surface motions are suggested for comparison with Earth data leading to an apparent need for magnetic coupling between the core and the mantle.

Key words: core energy, core–mantle coupling, Earth's core, geodynamo, precession.

1 INTRODUCTION

Progress in research on lunisolar precession of the mantle and its possible effect on motion in the liquid core and maintenance of the geodynamo has been uneven over at least a century. Studies were begun by Hough (1895) and Poincaré (1910), who included a solution of liquid motion, equivalent to the first term in a series expansion, as flow with constant vorticity, i.e. a rigid body component of motion. Later Busse (1968) extended global analyses by Bondi & Lyttleton (1953) and by Roberts & Stewartson (1965) to include non-linearities. Tentative acceptance of Poincaré's first term as representing the entire solution for a nearly spherical cavity, supported by the intrinsic two-dimensionality of rotating fluids (Greenspan 1968), led to the rigid-sphere model of Vanyo & Likins (1972) for net liquid motion and for energy dissipation as an exercise in Eulerian rigid-body dynamics. Although the Busse solution leads to equivalent expressions, Vanyo & Likins (1972) provides equations expressed in variables easily accessible to measurement during experiments. Research on precession within a geophysical context diminished in the mid-1970s with the publication of several papers critical of its adequacy to power a geodynamo, e.g. Rochester *et al.* (1975) and Loper (1975). During the same period, aerospace research on liquids in precessing objects accelerated. Because of persistent difficulties in seeking rigorous analytical solutions, much of that research relied on carefully scaled experiments.

By 1980, in addition to the early experiments by Malkus (1968), that indicated a potential for large energy dissipation rates, and by Vanyo & Likins (1971) that reported dissipation rates over a wide range of parameters in a nominally spherical cavity, a large body of relevant research had been published in the aerospace literature. Vanyo & Paltridge (1981) made use of this aerospace experience and examined application of the rigid-sphere model to the Earth's core to assess permissible energy dissipation magnitudes. Their paper included application of Paltridge's studies of possible multiple steady states for climatic conditions in the Earth's atmosphere to potential multiple steady-state dissipation patterns within the Earth's core. Vanyo (1984) continued this line of research and reported experimental energy dissipation rates in cavities with ellipticities of $+1/55$, $+1/400$ and $-1/400$ with the $+1/400$ oblate cavity tested in both smooth-walled and rough-walled versions. Viscous coupling to a smooth cavity wall was compared with pressure force coupling due to ellipticity and also to the presence of surface irregularities (small bumps) on the cavity surface. This research achieved Ekman numbers of $\sim 10^{-7}$ and refined estimates leading to a proposed core–mantle 'equivalent' Ekman number $\sim 10^{-10}$, a boundary layer $\sim$50 m thick and a westward drift of $\sim 0.2^\circ$ yr^{-1}. A paper by Vanyo (1991) directly addressed the question posed by Rochester *et al.* (1975) in their manuscript, i.e. 'Can precession power the geomagnetic dynamo?' This paper (i.e. Vanyo 1991) did not advance a more satisfactory theoretical description, but attempted only to show that precession could power a geodynamo. The paper included additional experimental evidence on energy dissipation and preliminary evidence of net liquid–cavity (core–mantle) relative motion during precession. Most tests met predictions of the rigid-sphere model within several per cent.

Experiments using a transparent 50 cm diameter globe with ellipticity of $\sim 1/100$ illustrated surface and interior flows by use of dyes injected at the surface during precession and by dispersed microscopic 'flakes' that defined shear surfaces (Vanyo *et al.* 1995). Spin and precession rates were varied from regimes of extreme turbulence to regimes of extremely stable laminar flow. Turbulent conditions exceed parameters in the Earth's core by orders of magnitude, indicating a non-turbulent core (in the absence of other forces) lagging the mantle in precession and with slow westward drift. Sets of concentric cylindrical interior flows were observed. Alternate cylinders have north–south and south–north internal flows with alternate cylinders also rotating slightly faster and slower than net averaged core rotation. Vanyo & Dunn (2000) continued examination of surface and interior flows but used a second transparent globe, again 50 cm in diameter but precisely manufactured to have a $+1/400$ ellipticity accurate to better than 20 μm. The mechanical strength and rigidity of the plastic globe and dye injection mechanisms limited the Ekman number to 2×10^{-7} and a Poincaré number (spin to precession ratio) of 10^6 compared with the Earth's 10^7. Surface flow and cylindrical interior flows were photographed and timed. Again, the rigid-sphere model accurately predicted net relative motion. This included liquid-cavity lag angle during precession, westward drift rate and surface flow patterns caused by misalignment of the axes. Application to the Earth was considered by matching the rate of energy dissipation needed for the geodynamo and by matching observed magnetic westward drift rate.

2 EQUATIONS: A REVIEW

Vanyo & Lods (1994) summarized an analysis for relative core–mantle motion with the core as a rigid sphere spinning at near the mantle rate but lagging the mantle axis in precession. Fig. 1(a) illustrates geometry and nomenclature. A cavity (mantle) spins at rate $\boldsymbol{\omega}$ while precessing with a half-coning angle θ at rate $\boldsymbol{\Omega}$ about an inertially fixed axis (n_3). An Eulerian three-angle relationship between a non-rotating frame (n for Newtonian) and an arbitrarily oriented mantle frame (m) uses rotation—about n_3 to the g frame, a rotation θ about g_1 to the e frame, and finally rotation $\boldsymbol{\omega}$ about e_3 to the mantle m frame.

Use of a 'rigid-sphere' model is not unique to the work of Vanyo and Likins. A similar model was used by Rochester *et al.* (1975, pp. 667 and 670), '*... the total core vorticity ξ is inclined to $\boldsymbol{\omega}$ ... by the small angle χ ... called the "tiltover".... It is sufficient to regard the core–mantle interface as spherical, and to represent the slip of the core past the mantle as $v = (\xi - \omega)\, xr$*' (their notation ξ and χ is not used here) and by Loper (1975, pp. 43 and 46), '*The relative orientation of the angular-velocity vectors of the mantle and core ... are determined from a torque balance.... For purposes of rotational dynamics, we may treat the entire Earth and the mantle and core individually as homogenous rigid bodies with spherical boundaries...*'

The angular velocity of the liquid sphere (core) relative to the precessing g frame ($\boldsymbol{\omega}^{\ell}$) in g frame components, from Vanyo & Likins (1972), is obtained by equating coupling torque to the change in angular momentum of the core. Routine solution yields

$$\boldsymbol{\omega}^{\ell} = -[\zeta/(1+\zeta^2)]\omega \sin\theta\, \hat{\mathbf{g}}_1 - [\zeta^2/(1+\zeta^2)]\omega \sin\theta\, \hat{\mathbf{g}}_2 + \omega\cos\theta\, \hat{\mathbf{g}}_3. \tag{1}$$

The dimensionless parameter ($\boldsymbol{\zeta}$) is

$$\boldsymbol{\zeta} = 5\nu/hR\boldsymbol{\Omega} \tag{2}$$

where ν is kinematic viscosity, h is an Ekman boundary layer thickness with characteristic size $(\nu/\omega)^{1/2}$ and R is the radius of the liquid sphere. The parameter $\boldsymbol{\zeta}$ is a type of Ekman number scaled to h, to $\boldsymbol{\Omega}$ and to R. It also represents a ratio of applied moment to inertial reaction of the (rigid) liquid sphere.

With the angular velocity of the core determined as a function of known parameters, the lag angle (tiltover), westward drift and energy dissipated are available. Lag angle β' is available from

$$\boldsymbol{\omega}^{\ell} \cdot \boldsymbol{\omega} = \omega^{\ell}\omega\cos\beta'. \tag{3}$$

Energy dissipation (power, P) at the interface (core–mantle boundary (CMB) for the Earth) is

$$P = [\zeta/(1+\zeta^2)]\mathbf{I}\Omega\omega^2\sin^2\theta \tag{4}$$

where $\mathbf{I}$ is the moment of inertia of the liquid sphere assumed to be rigid.

The velocity of the liquid surface relative to the cavity at each point $P(\delta, \lambda)$ was derived by Vanyo & Lods (1994) as an exercise in spherical trigonometry. Here δ is cavity latitude (north and south), λ is longitude (east and west) from the plane containing $\boldsymbol{\omega}$, $\boldsymbol{\omega}^{\ell}$ and $\boldsymbol{\omega}^{\ell m}$, and β is the latitude angle of $\boldsymbol{\omega}^{\ell m}$ (see Fig. 1). As with the work of Rochester *et al.* (1975)

$$\mathbf{V}^{\ell m}(\delta, \lambda) = \boldsymbol{\omega}^{\ell m} \times \mathbf{R} \tag{5a}$$

where

$$\boldsymbol{\omega}^{\ell m} = \boldsymbol{\omega}^{\ell} - \boldsymbol{\omega}. \tag{5b}$$

As scalar magnitude and direction

$$V^{\ell m}(\delta, \lambda) = \omega^{\ell m} R \sin\sigma \tag{5c}$$

with

$$\sigma = \arccos(\cos\beta\cos\delta\cos\lambda - \sin\beta\sin\delta). \tag{5d}$$

The angle between $\mathbf{V}^{\ell m}$ and a parallel of latitude at (δ, λ) is

$$\gamma(\delta, \lambda) = \pi - \arcsin(\cos\beta\sin\lambda/\sin\sigma). \tag{5e}$$

The model equations for $\boldsymbol{\omega}^{\ell}$ and for P accurately predict real flows as verified by numerous experiments and applications. The equations for $V^{\ell m}(\delta, \lambda)$ and $\gamma(\delta, \lambda)$ provide correct magnitudes but require caution to verify the correct quadrant over the entire range of (δ, λ). These may be compared with equivalent results obtained in an alternative format by Pais & Le Mouël (2001).

3 CORE MOTION

Fig. 2(a) illustrates a liquid spin axis lagging the mantle axis in precession by an angle β'. The relative angular velocity ($\boldsymbol{\omega}^{\ell m}$) is displaced by an angle β below the mantle equator. In general $\beta \neq \beta'$, e.g. if $|\boldsymbol{\omega}^{\ell}| = |\boldsymbol{\omega}|$, then $\beta = \beta'/2$ as in Fig. 1(b). These orientations are fixed in the Earth's precessing frame (g) that rotates once each 25 800 yr. Precession $\boldsymbol{\Omega}$ torques the liquid sphere and provides a basis for the lag angle β', but in other matters $\boldsymbol{\Omega}$ will be additive with spin rate $\boldsymbol{\omega}$, a ratio of 10^{-7} for the Earth, and is neglected. Polar circles are drawn about the $\boldsymbol{\omega}^{\ell m}$ axis such that $V^{\ell m}(\delta, \lambda)$ are given by eq. (5c). A rotated view is included as Fig. 2(b) to further illustrate intersection angles between the $\omega^{\ell m}$ polar circles and meridians of longitude of the mantle. Applied to the Earth, this pattern of relative velocities is essentially fixed in space (rotating only at the precession rate), and the mantle and the liquid rotate past it each day with the liquid rotating a little slower. Except for a unique $\boldsymbol{\omega}^{\ell m}$ aligned so that $\beta = 0^{\circ}$, a westward component of velocity exists at each longitude along the equator as seen in Fig. 2(a). At higher latitudes, the motion is more complex. At 45° latitude, as seen in Fig. 2(b), velocity changes from northwest at 90°E to northeast at 120°E.

To aid in interpreting Figs 2 and 3, assume there is an observer stationary on the mantle at some latitude δ. As the mantle and core rotate counter-clockwise (viewed from the north), the observer is carried successively through the relative velocity pattern

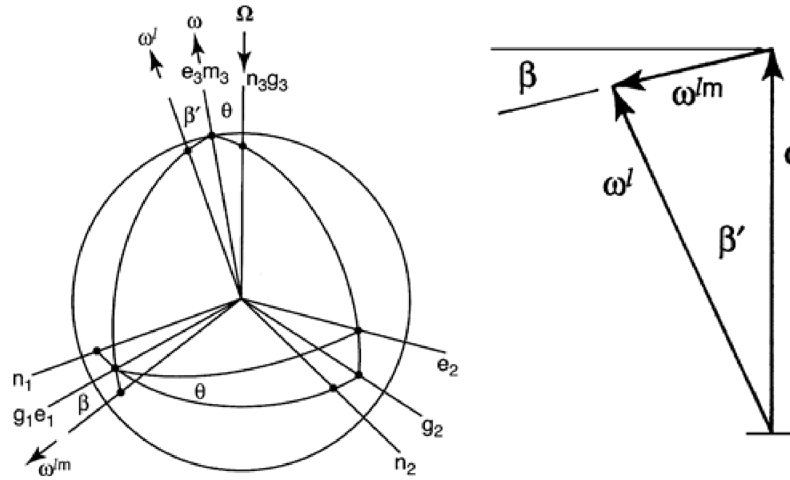

Figure 1. (a) Applied to the Earth, the mantle (m) spins at rate $\boldsymbol{\omega}$ (in g frame components) about its polar m_3 axis while precessing at rate $\boldsymbol{\Omega}$ about the ecliptic axis (n_3) at angle $\theta = 23.5°$. For the nearly spherical core–mantle boundary, with $\boldsymbol{\omega} \gg \boldsymbol{\Omega}$, the liquid core responds as a nearly rigid sphere spinning at a rate $\boldsymbol{\omega}^{\ell}$ and lagging behind the mantle in precession by a small angle β'. The angular velocity of the liquid relative to the mantle is $\omega^{\ell \mathrm{m}}$ at angle β as shown. (b) The vector diagram shows $|\boldsymbol{\omega}^{\ell}| = |\boldsymbol{\omega}|$ for which $\beta = \beta'/2$.

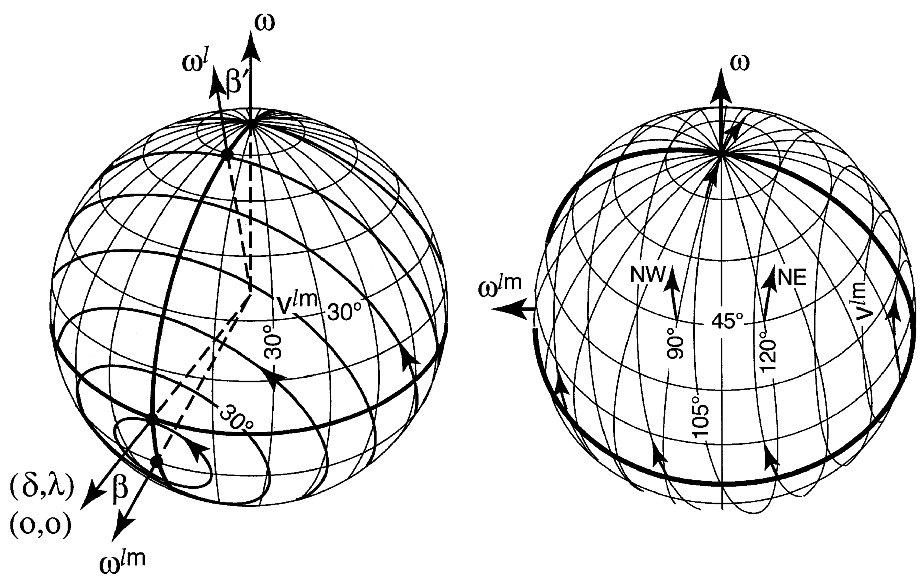

Figure 2. (a) Angular velocity of the liquid core relative to the mantle is computed as ($\boldsymbol{\omega}^{\ell \mathrm{m}} = \boldsymbol{\omega}^{\ell} - \boldsymbol{\omega}$). Polar circles, at angle $\boldsymbol{\sigma}$ to $\boldsymbol{\omega}^{\ell \mathrm{m}}$, are shown against a latitude–longitude grid coincident with the mantle axis and equator. Here, the prime meridian is fixed in the precessing (g) frame, not on the spinning mantle. (b) A rotated view of (a) shows the polar circles change from westward to eastward flow (and back) at mid-latitudes as the mantle/core rotate past the fixed pattern of $V^{\ell \mathrm{m}}(\delta, \lambda)$.

$V^{\ell \mathrm{m}}(\delta, \lambda)$ at the spin rate of the Earth. The observer will 'see' the core beneath, with this relative motion, at each λ. If the observer starts at $(\delta, \lambda) = (0°, 0°)$ and identifies a specific spot (A) on the core, the observer will see the spot there moving directly westward. After 6 hours, the observer will have moved with the mantle 90° eastward and will see nearly vertical motion of the core. After 12 hr ($\lambda = 180°$), relative motion is again directly westwards finally moving southwards to the starting point after 1 day. The curve in Fig. 3 for ($\delta = 0°$) is an integral of $V^{\ell \mathrm{m}}(\delta, \lambda)$ over λ continued for 3 days.

When δ is chosen equal to β, the curve has a pole-ward cusp, and at even higher latitude the curve 'folds over' to form sets of overlapping anticyclonic (northern clockwise) swirls. For example, imagine the observer at $(\delta, \lambda) = (45°, 0°)$. Core motion is initially westward relative to the mantle as shown in Fig. 2(a), but as seen in Fig. 2(b), when ($\lambda = 90°$) motion is northwest and when ($\lambda = 120°$) motion is northeast, having just passed an inflection point in the curve. At ($\lambda = 180°$), core motion is now directly eastwards, returning on the far side of the globe to the southeast then southwest and finally after 1 day returning again to a westward direction, having completed one anticyclonic loop.

In Fig. 3, the diagram of relative motion for $\beta = 3.8°$ is expanded as sets of separate curves for mantle latitudes at each 15°. In each set, relative motion is continued over three spin cycles (days). The sets for latitudes 0°, 3.8° and 15° are similar in wave shape and wavelength, essentially vertical oscillations with slow westward drift. The sets of $\delta = 75°$ and 90°, as a group, define mostly circular flows, while the sets of $\delta = 30°$, 45° and 60° can be approximated as elliptical with a wavelength and shape of about the 45° set. All loops shown form in a clockwise sense, i.e. anticyclonic for

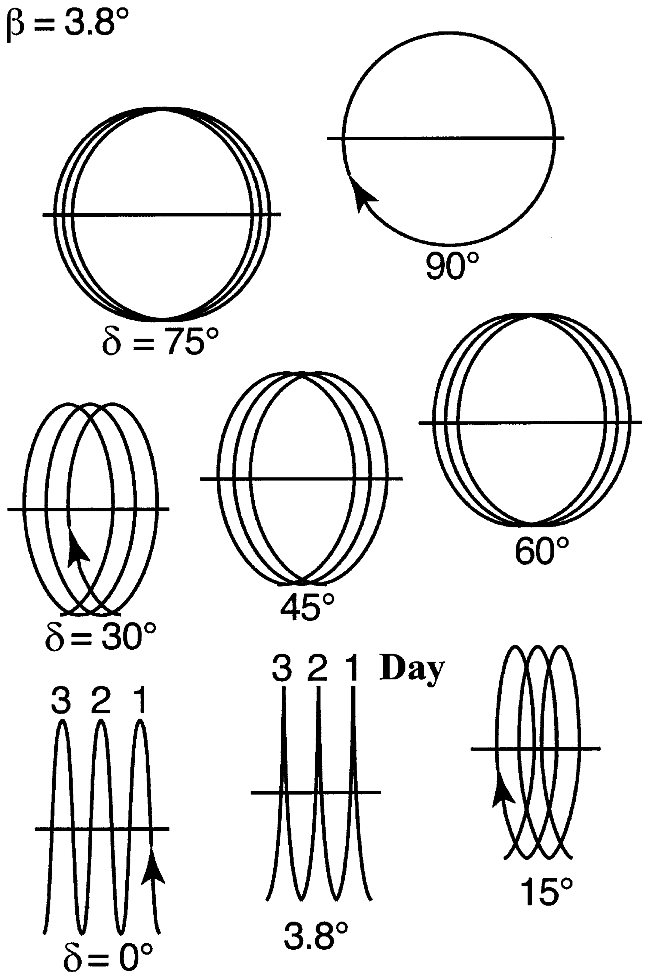

Figure 3. Curves illustrating core–mantle relative motion are separated for each 15° of latitude and are shown continued for three cycles (days). The value of $\beta = 3.8°$ compares with the experiments of Vanyo & Dunn (2000). Relative motions for latitudes 0°, 3.8° and 15° average out as a group to mostly vertical oscillations with westward drift. Those at 30°, 45° and 60° average to elliptical motion with a lesser westward drift, and those at 75° and 90° approximate circular relative motion.

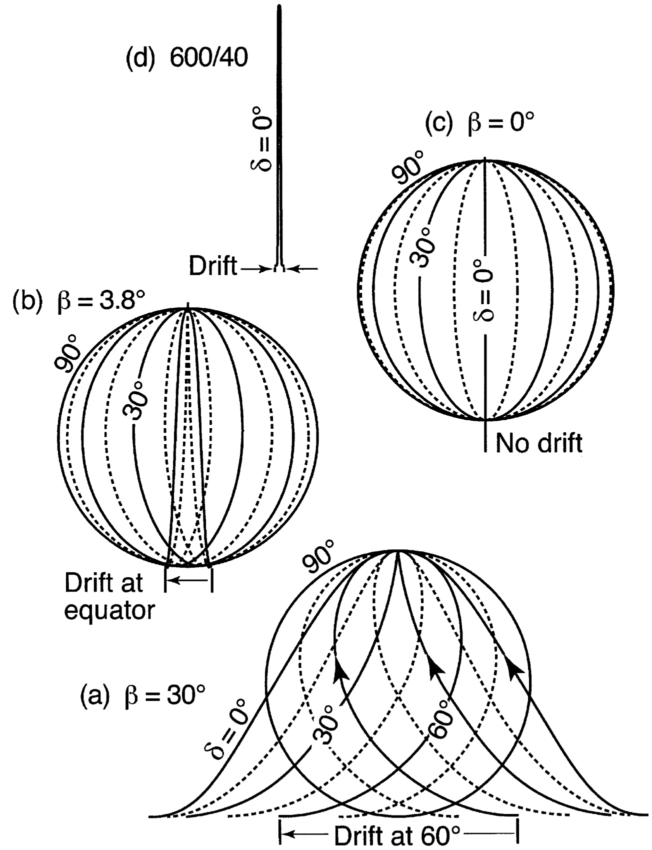

Figure 4. Four values of β are shown with all curves aligned at their $\lambda = 180°$ symmetry axis. (a) A value of $\beta = 30°$ is not realistic in nature or in the laboratory, but it illustrates the dependence of wave height on β' and westward drift on β. (b), (c) Show β of 3.8° and 0° respectively. Each set of curves shows relative motion, core to mantle, at each 15° of latitude over one daily cycle. (d) shows relative displacement, at the equator only, of a suggested Earth model with 600 m displacement of axes at the CMB and 40 m daily westward drift at the equator; at higher latitudes, the curves approach those of $\beta = 0°$.

northern hemisphere motion. Actual flows will be expected to integrate these patterns. They should not be expected to reproduce any of the calculated sets of profiles exactly for several reasons:

(1) Profiles, as a function of latitude, change shape continuously from equator to pole, and each set of profiles overlap by a magnitude β' with those above and below. In addition, profiles at adjacent longitude vary continuously in phase.

(2) Net westward flow is smoothly continuous at the equator and circular flow is smoothly continuous near the pole, but elliptical patterns at mid-latitude include both eastward and westward motions that are much larger than their net westward motion. Zonal displacement approximates meridional displacement, and both should be expected to obfuscate any simple or clean elliptical pattern, at best resulting in a continuously changing or partially turbulent flow.

(3) An observer would see an effect similar to that obtained by translating a sheet of glass in an elliptical or circular pattern over a flat surface covered with sand or coarse grease. The glass translates in that pattern; it does not rotate and the motion is small compared with the area of the glass. For northern hemisphere simulation, the centre of clockwise motion moves slowly left. Observation is greatly augmented by introduction of a tracer fixed to the fluid, e.g. an injection of dye in an experiment or a magnetic field anomaly at the CMB.

The calculated relative motion curves in Fig. 3 can be compared with the experiments of Vanyo & Dunn (2000) in which dye tracers were injected during steady-state precession equivalent to the values used to calculate Fig. 3. All values were held to an accuracy of 1 per cent or better, and these experimental simulations (solutions) of precession under given conditions probably represent reality better than any current analytical or computer solutions. There is no avoidance of non-linear terms, viscous coupling, ellipticity or round-off errors, etc.

Fig. 4 compares relative motion curves for four values of β to illustrate the dependence of westward drift on β. The curves in Fig. 4 all have retrograde motion and are generated right to left as indicated by the arrows. All loops shown are generated with clockwise motion, i.e. anticyclonic. Curves for all latitudes are shown aligned at $\lambda = 180°$ to aid shape comparison. All curves are normalized to the same value of β' to help demonstrate that β' determines the amplitude of the relative motion while β determines the wavelength (westward drift). As noted by Pais & Le Mouël (2001), motion of a fixed point on the liquid relative to the mantle (a pathline) during one spin cycle would appear slightly different, especially if the relative motion were large, but with a total probable angular displacement β' of the order of 0.01°, the difference is negligible for the Earth. More precisely, the curves represent drag force of the liquid against the mantle at that latitude. A magnetic field line embedded in the conducting liquid but restrained by a less conducting lower mantle will be stretched and dragged transversely in this pattern. Dye injected into a boundary layer during precession will permeate the layer and be dragged along the cavity surface in a similar pattern. Northern hemisphere motions are shown. Southern motions are mirror images displaced 180° in λ.

A value of $\beta = 30°$ is difficult to achieve in the laboratory and results in intense interior turbulence as seen in Vanyo *et al.* (1995). It is not relevant to Earth motions, but the calculation helps to illustrate features of relative motion as a function of latitude. The defining latitude for each curve is at its north–south midpoint. At the equator ($\delta = 0°$) motion is approximately sinusoidal, shown as one cycle from southernmost to southernmost. At $\delta = 15°$ (dashed line), the 'sinusoidal' shape distorts to be narrower at the poleward edge, reaching a cusp at $\delta = \beta = 30°$. Above $\delta = 30°$, the curve 'folds over' to form a loop with greater net westward motion than eastward. At higher latitudes the curves are more elliptical, becoming circles at the pole. Because westward drift represents motion of one sphere to another, the net linear westward drift is maximum at the equator and zero at the pole. Circular motion near the pole demonstrates the dependence of amplitude on β'. The amplitude at all latitudes is $2\beta' R$.

The set of curves for $\beta = 3.8°$ compare well with the Vanyo & Dunn (2000) experiments using a precisely machined 50 cm diameter cavity with ellipticity $\varepsilon = 1/400$, filled with de-aired distilled water and spinning at 200 rpm, with $\theta = 23.5°$, and precessing with a 10 min period. Values of β' and westward drift matched rigid-sphere computations within a few per cent. The curves labelled $\beta = 0°$ show the limit as $\beta \to 0°$. Westward drift is zero and motion at the equator is a vertical oscillation, but again transforming to circular motion at the poles (see also Fig. 6 in Pais & Le Mouël 2001).

Vanyo (1991) suggested that a displacement of the liquid and mantle axes at the CMB of 600 m (35 arcsec misalignment of axes) and a westward drift of 40 m day^{-1} at the CMB equator might be reasonable values for discussion of Earth phenomena. One cycle (1 day) of relative motion at the equator is drawn to scale in the curve labelled 600/40. Motion at higher latitudes has a westward drift which is too small to illustrate at this scale, but it is approximated well by the $\beta = 0°$ curves. A 600/40 model for the Earth indicates total daily relative motion of each point on the equator to be 2400 m north–south plus the 40 m day^{-1} drift. Total daily displacement near the pole is approximately $1200\pi = 3700$ m.

Fig. 5 includes photographs of observed surface flows. Injected dyes shown in Fig. 5(a) from Vanyo & Dunn (2000) show the flow pattern in the polar region to be circular from about 70° latitude to the pole, i.e. a 40° included angle. Note especially the filament of red dye injected at 60° that has migrated northward until it is 'captured' by the circular flow. Circular flow forcing is too intense to permit meridional flow poleward of 70° in the experiment. Figs 5(b,c) from similar experiments include flow patterns nearer the equator. The patterns show tips of approximate sine waves with a new tip generated each spin cycle corresponding to the low-latitude profiles of Fig. 3. Westward distance between the tips is the calculated wavelength (westward drift per cycle). The tips grow in amplitude to approximately 30° latitude. Diffusion and mixing obliterate the central portion of the pattern.

All photographs show portions of mid-latitude surface flow. Precise ellipses are never seen, instead a plurality of slowly changing nearly circular and wavy patterns appear and disappear. Nearly elliptical patterns with anticyclonic rotation are seen in Figs 5(a,b). Fig. 5(c) shows latitudinal bands of convergence (concentrations of surface dye) and divergence (dispersal of dye). Other photographs in Vanyo & Dunn (2000) show cross-sections of the globe some time after distribution of surface dye and its flow into the interior. The cylinders with downward-moving dye align with latitudinal bands of dye as in Fig. 5(c). Alternate cylinders flow upwards, bringing clear water to the clear latitudinal bands. What is finally seen in the experiments is often a function of how and where dye is injected and the elapsed time after injection. For example, Fig. 5(d) shows a trajectory of dye in the boundary briefly after injection at 60°N. Note that the other photographs show an integrated effect of dye injection over thousands of spin cycles, e.g. 20 min × 200 rpm (compare with 10 yr × 365 days yr^{-1}). Sometimes velocity profiles are made visible, at other times pathlines, streamlines, streaklines or timelines. Those terms, as used here, are defined in Vanyo (1993) (Dover edition, p.43). Addition of a solid inner core has been studied experimentally. The presence of a 'tangent cylinder' that effectively limits exchange of fluid to or from regions above and below the inner solid core is observed. More finely divided cylinders are seen within the tangent cylinder.

Voorhies (1995) (his Fig. 3 (centre)) and Matsushima (1995) (his Fig. 3a) present figures (see Fig. 6) showing core surface velocity fields derived from surface geomagnetic data observed over decadal timescales. These figures are in qualitative agreement. Both show continuous westward drift at and near the equator, large gyres at mid-latitudes, north and south, each spanning some 30° of latitude and longitude and with anticyclonic rotation, less distinct smaller gyres and random wave structures. At the poles both papers depict similar surface flows. An inertially fixed observer, as represented by the photographs, sees unidirectional flow past the cavity (mantle) pole. An observer, fixed to and rotating with the mantle will see this as a rotating flow. All are in conformance with photographs of surface flows using dye tracers and the predictions shown in Figs 3. and 4 of this paper. They can only be in general conformance as noted earlier and as analysed by Pais & Le Mouël (2001), but important features do correspond in each case. Any non-zero value of β provides continuous westward drift at equatorial latitudes in the calculations, in the experiments and in the magnetic field observations. All three indicate anticyclonic gyres (elliptical swirls) at mid-latitudes as in Fig. 3. An observer watching an experiment in real time sees these, but they are less obvious in photographs in which complex patterns appear and disappear as dye is advected.

As predicted by Vanyo & Lods (1994), '*. . . magnetic core–mantle coupling. . .generates magnetic vorticity at the MCB, maximized at the poles and minimized at the equator. A small magnetic retrograde drift exists everywhere.*' We did not predict that vorticity might coalesce flux mostly into several large gyres in each hemisphere, although that result is consistent with vortex theory. The estimates of Voorhies (1995) and of Matsushima (1995) use the property that a magnetic anomaly will remain fixed to the same particles of any fluid with high electrical conductivity. Fluid vortices in a nearly inviscid fluid have a similar property of remaining with the same fluid particles. Parallel vortices with the same rotation sense have an additional property that they will rotate each other about their vortex centroid in much the same way the Earth and Moon orbit about their common centre of mass.

Although small and rapid field disturbances are presumably too weak and/or too fast to penetrate the mantle without dispersion

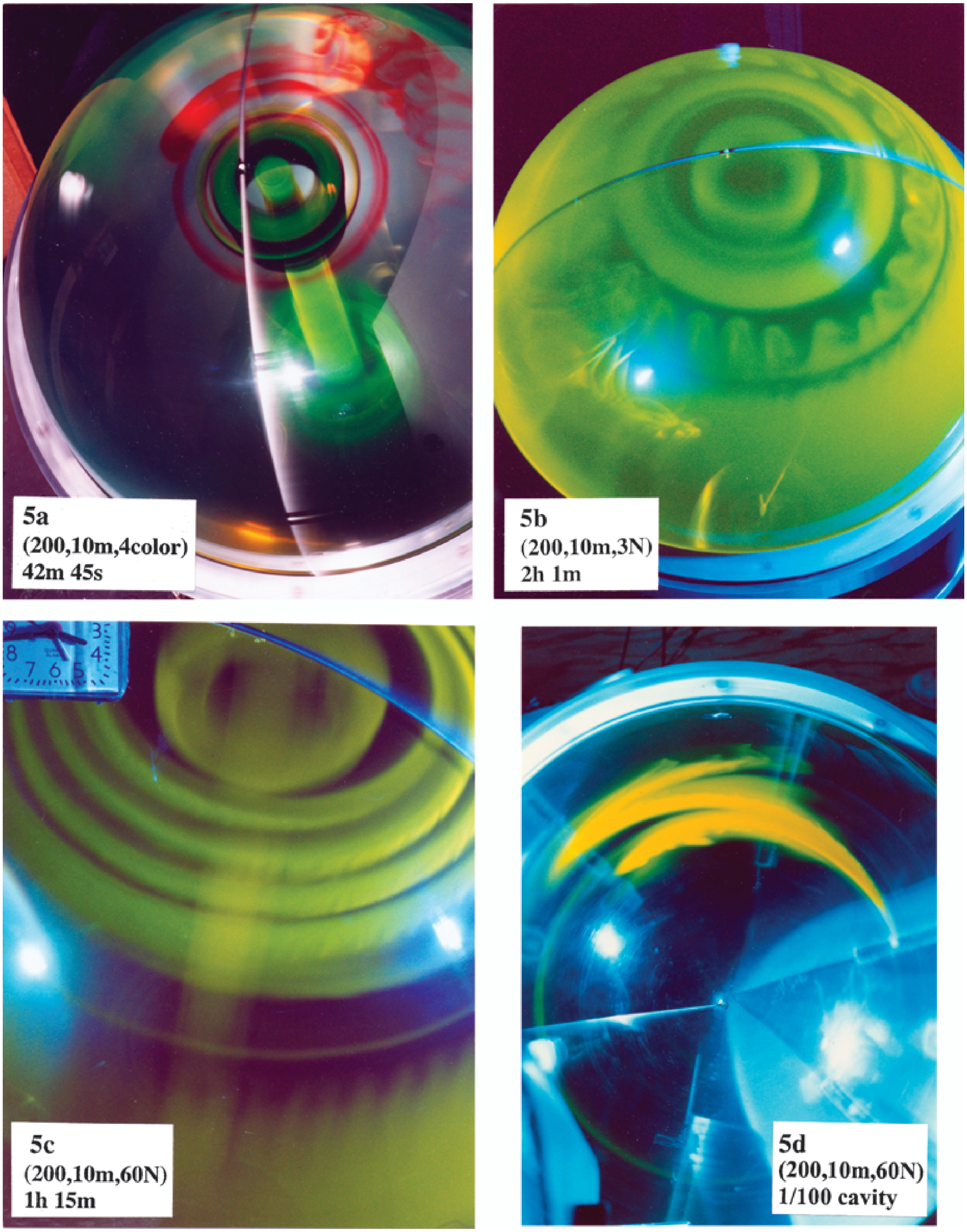

Figure 5. Photographs illustrate advection of dyes in a transparent 50 cm diameter globe with 1/400 ellipticity filled with water and spinning at 200 rpm with $\theta = 23.5°$. Labels indicate the spin rate in rpm, precession period in minutes, latitude of injection and time after injection. Parts (a), (b) and (c) are from Vanyo & Dunn (2000). Four dyes are injected impulsively to pierce the boundary layer in (a), black at 90°N, yellow at 90°S and red at 60°N. Blue at 30°N is not seen here. In parts (b), (c) and (d) yellow dye was slowly injected into the boundary layer for 1 to 2 s. Circular polar flow is seen in (a), (b) and (c). Mid-latitude 'elliptical' swirls are seen in (a) and (b), and tips of sinusoids are seen in flows nearer the equator in (b) and (c). Part (d), from a different experiment with 1/100 ellipticity, illustrates the initial trajectory of dye injected into the boundary at 60°N. Latitudinal bands rotating faster and slower than net ω^{ℓ} cause the jagged appearance in (d). Dye will later concentrate as in (c), later to be advected into interior cylinders. The globe spins counter-clockwise and precesses clockwise in all photographs.

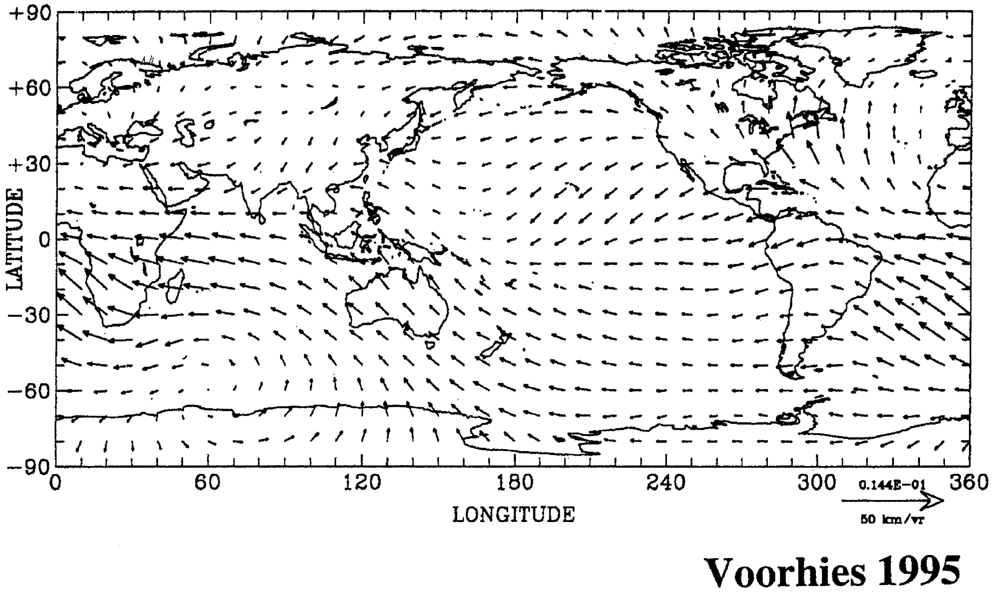

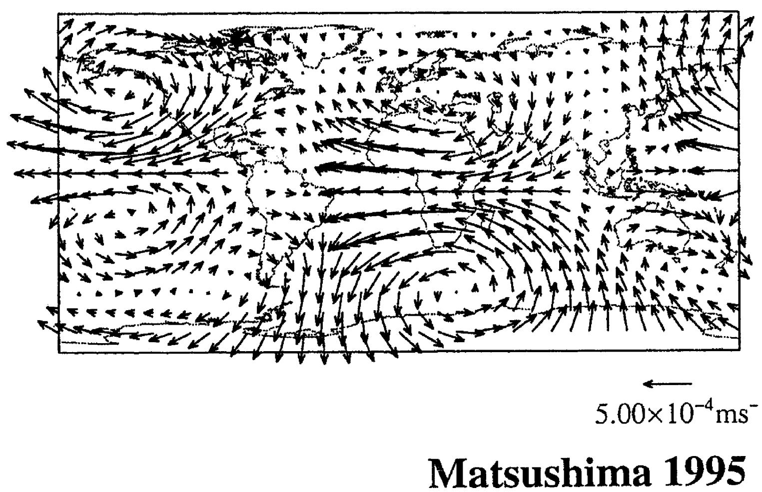

Figure 6. Flow patterns at or near the CMB estimated from geomagnetic field models—top drawing from Voorhies (1995), bottom drawing from Matsushima (1995). Each is an estimate of surface flow at the core–mantle boundary using a 'frozen field' assumption that horizontal components of magnetic field at the CMB represent similar flows of conducting fluid (see references for details).

and/or dissipation, they do have a potential for creating observable features if repeated daily for thousands of years. A small viscosity will cause small separate fluid vortices to coalesce into one large vortex. A distribution of small-diameter relative motion loops generated at the CMB over thousands of days (say even 10 yr) will have random encounters as they move westwards and begin to coalesce into larger and larger vortices. The phenomenon can also be evaluated using Stokes' theorem that vorticity integrated over a closed surface is equal to circulation around its periphery. Magnetic field anomalies carried by these larger vortices will be seen as magnetic vortices moving slowly westward with anticyclonic rotation, as seen in the charts of Voorhies (1995) and Matsushima (1995). Their figures, if steady state, infer a quasi-steady state of vorticity generation and its dissipation by viscosity and possible magnetic field generation.

Similar coalescence of vortices is observed in nature and in engineering: for example large cyclonic thunderstorms that form in the eastern Atlantic in the summer coalesce into hurricanes as they follow the trade winds westward, and lifting wing vortices shed along the length of a tapered wing coalesce with the tip vortex to form a single vortex just inboard of the tip—behind the aircraft this vortex reacts with the opposite wing vortex, with each then forcing the other downwards. Details of vortex merging are analysed by Cerretelli & Williamson (2003).

Holme & Whaler (2001) examine core flows in a reference frame that is allowed to rotate relative to the mantle. Their base analysis yields a frame drifting westwards at about the observed $0.2^\circ\ \mathrm{yr}^{-1}$ drift of the magnetic field. When a more complex flow is analysed, they obtain two solutions, one westwards and one eastwards, although the second solution provides '*only a small additional misfit reduction*'. Mid-latitude flows similar to the ellipses of Figs 3 and 4 might be expected to appear in calculations as both westward and eastward drifts.

4 ENERGY ESTIMATES

Any selection of β and β' infers also a corresponding quantity of energy dissipation. Equation (4) defines energy dissipation rate (power) in a liquid filled sphere during precession as

$$P = [\zeta/(1+\zeta^2)]\mathbf{I}\Omega\omega^2 \sin^2\theta. \tag{4}$$

For the Earth $\mathbf{I}\Omega\omega^2 \sin^2\theta \sim 6\times10^{16}$ W, and $\zeta/(1+\zeta^2)$ has a maximum value of 1/2 at $\zeta = 1$. Depending on the value for ζ, mantle precession could dissipate by as much as (3×10^{16} W) , a quantity far in excess of evidence. In the derivation, $\zeta = 5\,\nu/hR\Omega$ originates as a type of Ekman number, and $h = (\nu/\omega)^{1/2}$ is the conventional Ekman boundary layer thickness. With $\nu \sim (10^{-6}\ \mathrm{m^2\ s^{-1}})$, as commonly assumed for core liquid at the CMB, $\zeta \sim 1$, and $P \sim P_{\max}$. This is not because of an error in ν or the equation for P. It states that core–mantle coupling must be increased above that value of molecular viscosity. Rochester & Crossley (1987) and Lumb & Aldridge (1991) have estimated ranges of (equivalent) viscosity much larger than $10^{-6}\ \mathrm{m^2\ s^{-1}}$.

Net heat loss from the Earth to space today is estimated at 4×10^{13} W (Sclater *et al.* 1980). P can be reduced to this value by increasing coupling by any mechanism equivalent to some 'effective viscosity', with a value approximately 10^6 times the molecular viscosity of the core material. Power needed to energize a geodynamo is estimated at from 10^9 to 10^{12} W (Rochester *et al.* 1975). P can be further reduced to 10^{11} W by increasing effective viscosity, ν, by an additional 10^5 times. Precessional energy obtained from Earth rotational kinetic energy is limited by estimates of secular deceleration of the Earth's spin rate by lunar and solar torques. Estimates of the number of days per year from 850 Ma and 360 Ma of 435 and 397 respectively all compute to an approximately 3.5×10^{12} W average continuous loss of rotational kinetic energy (see Wells 1963; Munk 1966; Vanyo & Awramik 1985). Although this energy also powers other phenomena (lunar orbit changes, oceanic and solid Earth tides), even 10 per cent placed into core energy is three times the minimum of 10^{11} W needed for the geodynamo.

Important aspects of precession include that it could generate 3×10^{16} W but routinely has not, and that its output is very sensitive to changes in precession rate, axis inclination and especially magnetic core–mantle coupling. Radioactive sources are needed to explain net heat loss to space if today's energy rates are typical of earlier rates.

5 DISCUSSION

Like research on precession in general, estimates of core–mantle coupling mechanisms and their relative magnitude have been uneven over the last century. It is difficult to accept a viscosity value large enough over $10^{-6}\ \mathrm{m^2\ s^{-1}}$ to obtain a reasonable energy dissipation rate based solely on molecular viscosity. Pressure torques based on ellipticity, surface roughness and boundary turbulence, alone or together, are also improbable as adequate coupling mechanisms, based on experimental evidence.

Large departures from sphericity can induce pressure forces adequate to cause a liquid to follow cavity motion during precession. This is seen in the Malkus experiments using an ellipticity of 1/10 as a hysteresis loop in torque (i.e. also in P). Gans (1973), as part of a master's programme with Vanyo, observed the same hysteresis phenomenon using circular cylinders (as rocket fuel tanks). We were never able to excite the same phenomenon in spheroids with ellipticities of 1/100 or less. P can be detected and distinguished for ellipticities of $\pm1/400$, one from the other, but the differences are not significant and they do not depart significantly from the response expected from a perfect sphere, especially for very slow precession rates.

That the CMB is nearly spherical can be visualized by drawing a 10 cm radius arc with line width of 0.25 mm. The ratio is 0.25 mm:10 $\mathrm{cm^{-1}} = 1/400$, and the entire CMB shape will fit within the thin line width of the circular arc. In experiments simulating core flow using spheroids with $\pm1/400$ ellipticity, the viscosity of the liquid appeared to provide the dominant coupling mechanism—not pressure forces due to ellipticity. It is reasonable to extend this experience also to the Earth's core and to state that core motion is dominated by some type of direct core–mantle drag at the CMB—not pressure forces due to ellipticity. Pressure forces (inertia waves) exist in the core but at such a low energy level they may be insignificant.

Vanyo (1984) tested for roughness by comparing tests using a polished cavity (1/400 ellipticity) with the same cavity 'roughened' with small lacquer 'bumps' both less than and slightly greater than the calculated Ekman layer thickness. A small increase in P occurred using the rough surface at high precession rates. Some photographs in Vanyo & Dunn (2000) appear to show insignificant low-intensity boundary turbulence at mid-latitudes. Neither surface roughness nor surface turbulence are adequate to explain coupling and energy dissipation in the 1/400 experiments carefully scaled to Earth parameters.

The 1995 core flow estimates of Voorhies (1995) and of Matsushima (1995), when compared with experiments and computations, argue for reliance on magnetic coupling incorporated into the energy equation as part of an 'equivalent' viscosity. The quantity ν then represents coupling also by magnetic field lines that couple the conducting core to a conducting layer in the lower mantle. Estimating magnetic coupling as a component of an 'equivalent viscosity' has difficulties in that magnetic coupling is neither isotropic, homogeneous nor uniform over the CMB. It can only represent a fairly crude approximation to integrated magnetic coupling over the CMB with the major contribution occurring at higher latitudes where field lines should be nearer to perpendicular to the CMB surface. Extrapolation of Earth surface magnetic observations to the Earth's interior may not 'see' deeper than the manner and rate at which the field is 'dragged' through a conducting layer in the mantle. Westward drift of the core will then occur at a slightly greater rate with the difference representing magnetic field deformation. A difference will help to resolve the difficulty reported in the Vanyo & Dunn (2000) paper reconciling estimates based on westward drift when compared with estimates based on energy dissipation.

Over the last three decades inner (solid) core accretion and liquid core convection have generally replaced precession as a probable geodynamo energy source, and only recently has precession been reconsidered—often in attempts to understand the role of ellipticity and inertia waves. Interest in inertia waves was initiated by the prediction in Bondi & Lyttleton (1953) of an instability at 30° latitude. That analysis has been confirmed, but the instability has not been apparent in experiments. A large series of instabilities (the nested cylinders) are seen, not yet explained by theory. Other precessional research has lagged, in part because of formidable mathematical difficulties and in part because of papers in the mid-1970s that erred in their estimates of energy dissipation. Although several defined a rigid-sphere model for energy, none solved the model explicitly, nor did they discover that it had already been solved by Vanyo & Likins (1972). Instead they used estimates extracted from earlier papers based on various and numerous approximations, leading to P being seriously underestimated and discouraging further studies. A statement that all precessional energy is dissipated in the boundary layer was also in error. As with spin-up from rest, all energy transferred from cavity to fluid is deposited in the boundary layer (as kinetic energy), later to be transferred to the internal fluid. Some energy, in each case, will dissipate within the viscous boundary—but not all.

The recent paper by Pais & Le Mouël (2001) has contributed to understanding core–mantle relative motion. The abstract in Vanyo & Lods (1994) and Figs 2, 3 and 4 here help to further that understanding and to correct several minor inconsistencies, e.g. zero westward drift requires $\beta = 0^{\circ}$, regardless of whether $|\boldsymbol{\omega}^{\ell}| = |\boldsymbol{\omega}|$. In other matters, they did not have access to Vanyo & Dunn (2000) which was still in press when their paper was prepared. Comparisons of their analyses with the 1/400 ellipticity experiments would have been more favourable. Although precessional energy has been a major criterion in use or non-use of precession as a viable geodynamo mechanism, the near absence of physical experiments or numerical studies to examine the matter is remarkable—perhaps because both are as difficult to accomplish as analysis is formidable.

6 CONCLUSION

This research provides evidence that relative motion between the core and mantle caused by the core lagging slightly behind the mantle in precession may dominate all other energy and flow mechanisms. Simple algebraic models provide solutions that predict measured and observed energy dissipation rates, surface relative motion and net interior flows in carefully scaled experiments. In the experiments, molecular viscosity provides surface coupling (drag), but in the Earth corresponding ratios of torque to inertia cannot be achieved with any reasonable molecular drag force. Analyses and experiments predict core surface flow patterns with features similar to core surface flows computed with a geomagnetic imprint, indicating correlation between core–mantle motion and magnetic field structures and arguing for a significant, and perhaps dominant, magnetic field core–mantle coupling mechanism.

Although an explicit geodynamo model based on mantle precession has yet to appear, recent research indicates a real potential for core flows and adequate energy for a precessionally driven geodynamo. Specifically, the descending and ascending nested cylinders, each with slightly different angular velocity, provide helicity satisfying a feature considered critical for geodynamo action, and magnetic flux traversing between the conducting core and a conducting layer in the lower mantle is twisted and stretched by core–mantle relative motion placing precessional energy directly into magnetic energy. As with geodynamo models based on turbulent convection, precessional boundary motions, with or without introduction of magnetic coupling, will best be advanced through numerical studies.

ACKNOWLEDGMENTS

The University of California aided completion of this research and support for its presentation. Several persons, including reviewers, have offered very helpful suggestions which are much appreciated.

REFERENCES

Bondi, H. & Lyttleton, R.A., 1953. On the dynamic theory of the rotation of the Earth: the effect of precession on the motion of the liquid core, *Proc. Camb. Phil. Soc.,* **49,** 498–515.

Busse, F.H., 1968. Steady fluid flow in a precessing spheroidal shell, *J. Fluid Mech.,* **33,** 739–751.

Cerretelli, C. & Williamson, C.H.K., 2003. The physical mechanism for vortex merging, *J. Fluid Mech.,* **475,** 41–77.

Gans, W.C., 1973. Measurement of energy dissipation in liquid filled precessing cylindrical cavities, *MS Thesis*, University of California, Santa Barbara.

Greenspan, H.P., 1968. *The Theory of Rotating Fluids*, p. 327, Cambridge University Press, Cambridge.

Holme, R. & Whaler, K.A., 2001. Steady core flow in an azimuthally drifting reference frame, *Geophys. J. Int.,* **145,** 560–569.

Hough, S.S., 1895. The oscillations of a rotating ellipsoidal shell containing fluid, *Phil Trans. R. Soc. Lond.*, **186,** 469–506.

Loper, D.E., 1975. Torque balance and energy budget for the precessionally driven dynamo, *Phys. Earth Planet. Int.,* **11,** 43–60.

Lumb, I.L. & Aldridge, K.D., 1991. On viscosity estimates for the earth's fluid outer core and core-mantle coupling, *J. Geomag. Geoelectr.,* **43,** 93–110.

Malkus, W.V.R., 1968. Precession of the earth as the cause of geomagnetism, *Science,* **169,** 259–264.

Matsushima, M., 1995. Velocity and magnetic fields in the earth's core estimated from the geomagnetic field, *Phys. Earth Planet. Int.,* **91,** 99–115.

Munk, W.H., 1966. Variation of the Earth's rotation in historical time, in *The Earth–Moon System*, pp. 52–69, eds Marsden B.G. & Cameron, A.G.W., Plenum Press, New York.

Pais, M.A. & Le Mouël, J.L., 2001. Precession-induced flows in liquid-filled containers and in the earth's core, *Geophys. J. Int.,* **144,** 539–554.

Poincaré, H., 1910. Sur la précession des corps déformables, *Bull. astr.,* **27,** 321–356.

Roberts, P.H. & Stewartson, K., 1965. On the motion of a liquid in a spheroidal cavity of a precessing rigid body, II, *Proc. Camb. Phil. Soc.,* **61,** 279–288.

Rochester, M.G. & Crossley, D.J., 1987. Earth's third ocean: the liquid core, *EOS, Trans. Am. Geophys. Un.,* **68,** 481–483.

Rochester, M.G., Jacobs, J.A., Smylie, D.E. & Chong, K.F., 1975. Can precession power the geomagnetic dynamo?, *Geophys. J. R. astr. Soc.,* **43,** 661–678.

Sclater, J.G., Jaupart, C. & Galson, D., 1980. The heat flow through oceanic and continental crust and the heat loss of the Earth, *Rev. Geophys. Space Phys.,* **18,** 269–311.

Vanyo, J.P., 1984. Earth core motions: experiments with spheroids., *Geophys. J. R. astr. Soc.,* **77,** 173–183.

Vanyo, J.P., 1991. A geodynamo powered by luni-solar precession, *Geophys. astrophys. Fluid Dyn.,* **59,** 209–234.

Vanyo, J.P., 1993. *Rotating Fluids in Engineering and Science*, Butterworth-Heinemann, London (see also 2001 edition (Dover, New York)).

Vanyo, J.P. & Awramik, S.M., 1985. Stromatolites and Earth-Sun-Moon dynamics, *Precamb. Res.,* **29,** 121–142.

Vanyo, J.P. & Dunn, J.R., 2000. Core precession: flow structures and energy, *Geophys. J. Int.,* **142,** 409–425.

Vanyo, J.P. & Likins, P.W., 1971. Measurement of energy dissipation in a liquid-filled, precessing, spherical cavity, *J. Appl. Mech.,* **38,** 674–682.

Vanyo, J.P. & Likins, P.W., 1972. Rigid body approximations to turbulent motion in a liquid-filled, precessing, spherical cavity, *J. Appl. Mech.*, **39,** 18–24.

Vanyo, J.P. & Lods, D., 1994. Mantle-core relative velocities in precessionally driven flows, *EOS, Trans. Am. Geophys. Un.,* **75** (April supplement), 120.

Vanyo, J.P. & Paltridge, G.W., 1981. A model for energy dissipation at the mantle-core boundary, *Geophys. J. R. astr. Soc.,* **66,** 677–690.

Vanyo, J.P., Wilde, P., Cardin, P. & Olson, P., 1995. Experiments on precessing flows in the earth's liquid core, *Geophys. J. Int.,* **121,** 136–142.

Voorhies, C.V., 1995. Time varying fluid flow at the top of earth's core derived from definitive geomagnetic reference field models, *J. geophys. Res.,* **100,** 10 029–10 039.

Wells, J.W., 1963. Coral growth and geochronometry, *Nature,* **197,** 948–950.